Two-dimensional probing of ground-state vibrational dynamics in porphyrin molecules by fs-CARS

ARTICLE *in* JOURNAL OF RAMAN SPECTROSCOPY · SEPTEMBER 2001

Impact Factor: 2.67 · DOI: 10.1002/jrs.741

7 AUTHORS, INCLUDING:

Reinhard Schweitzer-Stenner
Drexel University
219 PUBLICATIONS **4,368** CITATIONS
SEE PROFILE

Wolfgang Kiefer
University of Wuerzburg
881 PUBLICATIONS **9,862** CITATIONS
SEE PROFILE

JOURNAL OF RAMAN SPECTROSCOPY
J. Raman Spectrosc. 2001; **32**: 771–784

JRS

Two-dimensional probing of ground-state vibrational dynamics in porphyrin molecules by fs-CARS

M. Heid,[1] S. Schlücker,[1] U. Schmitt,[1] T. Chen,[1] R. Schweitzer-Stenner,[2] V. Engel[1] and W. Kiefer[1]*

[1] Institut für Physikalische Chemie der Universität Würzburg, Am Hubland, D-97074 Würzburg, Germany
[2] Department of Chemistry, University of Puerto Rico, Rio Piedras Campus, P.O. Box 23346, San Juan, Puerto Rico 00931, USA

Received 2 February 2001; Accepted 18 April 2001

We report on spectrally dispersed femtosecond time-resolved coherent anti-Stokes Raman scattering (CARS) for the investigation of the electronic ground-state vibrational dynamics of porphyrin molecules in solution. The two-dimensional experimental data obtained in our measurements provide a detailed mapping of the large number of molecular vibrations in these systems, excited by broadband ultrashort laser pulses, and make a thorough interpretation of the complex signal structure possible. In particular, an analysis of the data by applying Fourier transform methods to the time domain signal allows a clear identification of the excited porphyrin normal modes when compared with results on the mode structure from spectrally resolved (cw) spectroscopy. Altogether the method is capable of yielding detailed information on the dephasing behavior and on the relative spectral positions of the excited vibrations at the same time. Three porphyrin systems, dissolved in dichloromethane, were investigated: magnesium octaethylporphyrin, magnesium tetraphenylporphyrin and the free-base porphyrin octaethylporphyrin. The measurements were performed in the spectral region of the ring vibrations of the porphyrin macrocycle. We also provide a discussion of the expected signals on a theoretical basis by deriving the CARS third-order non-linear polarization for these experiments.

INTRODUCTION

Femtosecond (fs) time-resolved spectroscopy has evolved into a highly diverse research field over the last decade which has opened up new exciting possibilities for the investigation of many interesting aspects of molecular dynamics in the ultrafast time regime.[1–5] However, despite the great variety of experimental techniques that has been developed, there are only a few methods that are capable of studying ultrafast molecular dynamics in the electronic ground state, one of which is the method of fs time-resolved coherent anti-Stokes Raman scattering (CARS).[6–21]

Generally, CARS is a four-wave mixing process involving three photons from the three incident laser beams pump, Stokes and probe, respectively, and the coherently scattered anti-Stokes photon. The method can be applied to either gain wavenumber-resolved or time-resolved information on the investigated sample. One of the major differences between fs-CARS and its cw/ns counterparts is that the fs time-resolved variant is performed in a pump and probe fashion with well-defined pulse sequences. To be able to probe electronic ground-state dynamics in our experiments, the excitation process consists of a stimulated Raman process involving the absorption of a photon from the pump pulse and the stimulated emission of a photon from the red-shifted Stokes pulse. This two-photon process generating a coherent ground-state vibrational excitation is highly flexible. Contrary to degenerate four-wave mixing techniques, for example, the excitation energy in the electronic ground state can be adjusted by the energy difference of the pump and the Stokes photon, making this method perfectly suitable for the selective excitation and probing of vibrational dynamics. Furthermore, the excitation can also be performed resonantly via an excited electronic state. In this case an additional time delay between the pump and the Stokes pulses might be introduced during which the amplitude generated by the pump pulse evolves unperturbed on the excited-state potential energy surface. For a diatomic molecule it has been shown that in this way the population transfer to a pre-chosen vibrational wave packet in the ground state can be optimized, and the internuclear separation at which the generation of the wave packet occurs can be controlled.[22,23] Other experiments

*Correspondence to: W. Kiefer, Institut für Physikalische Chemie der Universität Würzburg, Am Hubland, D-97074 Würzburg, Germany. E-mail: wolfgang.kiefer@mail.uni-wuerzburg.de
Contract/grant sponsor: Deutsche Forschungsgemeinschaft.
Contract/grant sponsor: Sonderforschungsbereich 347;
Contract/grant number: Teilprojekt C2 and C5.
Contract/grant sponsor: Fonds der Chemischen Industrie.

DOI: 10.1002/jrs.741

have shown that similar excitation processes can also be used to excite selectively different vibrational normal modes in a polymer.[24]

The goal of the present experiments was to apply fs time-resolved CARS spectroscopy successfully to the investigation of the electronic ground-state vibrational dynamics of large, biologically relevant molecules. Two problems are expected to arise when performing these measurements. The first originates from the fact that these systems usually have to be investigated in solution. In this case, the resonant isotropic scattering contribution containing the vibrational dynamics of the molecular system in which one is interested is often obscured by a considerably stronger non-Raman resonant scattering background from the solvent. This effect is particularly disadvantageous because of the restricted lifetime of the coherently excited ground-state population compared with experiments with small isolated molecules, and leads to a situation where the overall decay behavior of the transient signal might be strongly affected. To overcome this problem, a special polarization arrangement for the four light beams can be employed.[9,10] Generally, different scattering contributions, i.e. the non-Raman resonant, the resonant anisotropic and resonant isotropic contributions, can be suppressed by one of the so-called magic angle polarization geometries. Evidently, the first geometry is of special interest in our experiments and allows us to detect almost background-free transient signals rendering pure vibrational dynamics of the dissolved sample.

The second aspect of which one has to be aware is the high density of normal modes in a large molecular system. This results in a coherent excitation of many vibrational modes by the broadband laser pulses used in fs-CARS and leads to a highly complex structure of the transient signals. Therefore, special care has to be taken in order to be able to give any reasonable interpretation of the recorded signal and the large amount of information that is available. Very recently we have reported on a fs time-resolved CARS experiment that has been performed on magnesium octatethylporphyrin (MgOEP) dissolved in dichloromethane.[25] In order to overcome the above mentioned difficulty, the coherent anti-Stokes transient signal has been detected spectrally dispersed resulting in a two-dimensional (time and wavenumber) data set. An analysis of these two-dimensional time domain data on the basis of Fourier transform methods has shown that the technique is capable of yielding detailed spectral information on the vibrational mode structure of the investigated system in addition to vibrational dephasing times that are readily deducible from the decay behavior of the transient signals. We have now used this method to perform detailed measurements on a set of different porphyrin systems (see Fig. 1) over a broad range of their normal-mode spectrum in the interesting spectral region of the modes of the porphyrin macrocycle.

THEORY OF SPECTRALLY RESOLVED Fs-CARS

Before we show and discuss in detail the experimental results we have obtained, we want to give a brief theoretical derivation of the CARS signal we have to expect from our fs-CARS measurements. Several reports concerned with the basic theory of fs time-resolved CARS have been published before.[7,9,16–21,26] In the following we want to concentrate on a description of fs-CARS considering the special situation in our experiments, where the anti-Stokes signal is recorded spectrally dispersed as a function of the delay time of the probe pulse. Furthermore, in this paper we mainly focus on the spectral information (and mode assignment) that can be deduced from our measurements by employing Fourier transform methods to the two-dimensionally recorded transient signal. For the sake of clarity we therefore do not take into account explicitly the vibrational dephasing behavior of the excited normal modes.

For the assumption of an optically thin medium, the experimentally detected CARS signal is completely described by the third-order contribution $P^{(3)}(t)$ to the time-dependent polarization $P(t)$ induced in the sample. Using perturbation theory to solve the time-dependent Schrödinger equation, the state vector describing the investigated system can be written as sum over states of order n:

$$|\psi(t)\rangle = \sum_{n=0}^{\infty} |\psi^n(t)\rangle \tag{1}$$

leading to an expression for $P(t)$ of the form

$$P(t) = \sum_{n,m=0}^{\infty} \langle \psi^n(t)|\mu|\psi^m(t)\rangle \tag{2}$$

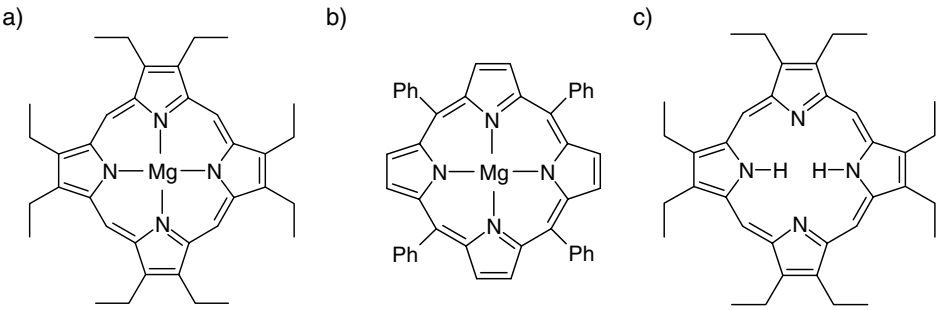

Figure 1. The Porphyrin molecules studied: (a) MgOEP; (b) MgTPP; (c) OEP.

where μ denotes the transition dipole moment which by neglecting all polarization directions at this point and using the Condon approximation is set to a scalar constant.

In our experiments, we detect the time-integrated spectrum of the CARS signal which is determined by the Fourier component at ω_{CARS} of the time-dependent third-order contribution to the induced non-linear polarization:

$$P^{(3)}(\omega_{CARS}) = \int_{-\infty}^{\infty} dt P^{(3)}(t) e^{i\omega_{CARS} t} \quad (3)$$

Generally, many different processes may contribute the to third-order non-linear polarization $P^{(3)}(t)$ in the CARS process. For our experiments it is reasonable to treat the investigated molecules as a model system consisting of two electronic states, $|X\rangle$ (ground state) and $|Q\rangle$ (excited state), which interacts with the three femtosecond laser pulses, pump, Stokes and probe, with wavevectors k_{Pu}, k_{St} and k_{Pr}, and center frequencies ω°_{Pu}, ω°_{St} and ω°_{Pr}, respectively. In what follows we consider transitions that start from the vibrational ground state in $|X\rangle$, neglecting rotational motion, and we employ the rotating wave approximation (RWA). Furthermore, we take advantage of the pulse sequence used in the experiment, i.e. the pump and the Stokes pulses are fired simultaneously and the probe pulse interacts with the system at positive delay times. We also take into account the wavelength arrangement and resonance conditions as shown in Fig. 2, leading to the requirement that the first photon has to be absorbed from the pump pulse. Finally, we use a folded BOX-CARS setup and a monochromator in the experiment which selects contributions emitted in the $k_{CARS} = k_{Pu} - k_{St} + k_{Pr}$ direction with center frequency $\omega_{CARS} = \omega^{\circ}_{Pu} - \omega^{\circ}_{St} + \omega^{\circ}_{Pr}$.

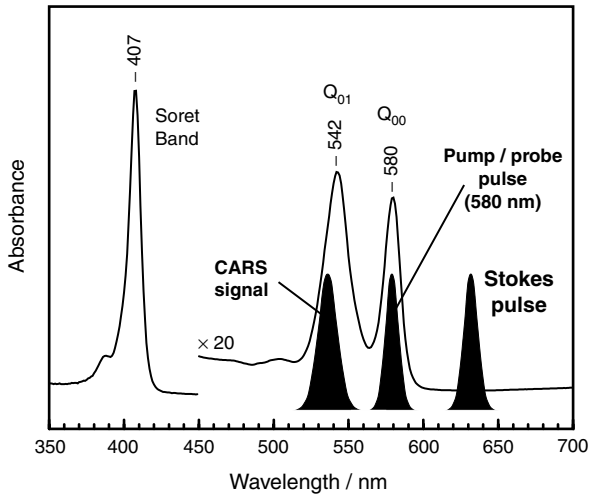

Figure 2. fs-CARS wavelength excitation scheme shown here for the case of MgOEP dissolved in dichloromethane. The absorption spectrum of MgOEP is expanded 20-fold in the *Q* band spectral region. A strong resonance enhancement of the CARS signal is achieved by tuning the pump/probe pulse wavelength to the absorption maximum of the Q_{00} band and by the location of the CARS signal in the vicinity of the Q_{01} band maximum.

Considering all these restrictions, we are left with only one contributing process to the experimentally detected CARS signal which correlates the unperturbed ground-state wavefunction $|\psi_0\rangle$ with the third-order state $|\psi^{(3)}_{Pu,St,Pr}(k_{Pu} - k_{St} + k_{Pr})\rangle$ and gives rise to the third-order non-linear polarization:[16,17]

$$P^{(3)}(t) = \langle\psi_0|\mu|\psi^{(3)}_{Pu,St,Pr}(k_{Pu} - k_{St} + k_{Pr})\rangle + c.c. \quad (4)$$

Using perturbation theory and employing light fields for the pump, Stokes and the probe pulse of the form

$$E_i(\mathbf{x}, t) = f_i(t - T_i) e^{-i\omega^{\circ}_i (t - T_i)} e^{+i\mathbf{k}_i \mathbf{x}} + c.c. \quad (5)$$

with Gaussian-shaped pulse envelopes $f_i(t - T_i)$, $P^{(3)}(\omega_{CARS})$ can then be rewritten from Eqns (3) and (4) as (atomic units are employed)

$$\begin{aligned} P^{(3)}(\omega_{CARS}) = -\left(\frac{1}{i}\right)^3 e^{-ik_{CARS}\mathbf{x}} \int_{-\infty}^{\infty} dt e^{i\omega_{CARS} t} \langle\psi_0|\mu \\ \times \int_0^t dt' U_Q(t - t')\mu f_{Pr}(t' - T_{Pr}) e^{-i\omega^{\circ}_{Pr}(t' - T_{Pr})} \\ \times \int_0^{t'} dt'' U_X(t' - t'')\mu f_{St}(t'' - T_{St}) e^{i\omega^{\circ}_{St}(t'' - T_{St})} \\ \times \int_0^{t''} dt''' U_Q(t'' - t''')\mu f_{Pu}(t''' - T_{Pu}) \\ \times e^{-i\omega^{\circ}_{Pu}(t''' - T_{Pu})} |\psi_0\rangle + c.c. \end{aligned} \quad (6)$$

where U_X and U_Q are propagators containing the Born–Oppenheimer hamiltonians of the electronic ground and the electronic excited state, respectively. The energy E_0 of the initial state has been set equal to zero so that the phase factor $e^{-iE_0 t'''}$ of $|\psi_0\rangle$ turns out to be equal to one. Intuitively, Eqn (6) can be interpreted in the following way: the unperturbed ground-state wavefunction $|\psi_0\rangle$ is first coupled to the excited state via the transition dipole moment μ by the external light field. The generated amplitude is then propagated in $|Q\rangle$ until the Stokes pulse stimulates an emission back to ground state $|X\rangle$, etc.

We now take account of the special situation of a high density of normal modes in our sample within the spectral width of the exciting laser pulses. In this case a large number of vibrational modes will be coherently excited when one of the pulses interacts with the system and it is therefore reasonable to employ a basis-set expansion with respect to the vibrational normal modes of the investigated system to the generated ground- and excited-state amplitudes. Furthermore, for the systems we are investigating, relaxation in the excited state occurs on a time-scale shorter than the pulse duration of our laser pulses. This point is based on experimental findings that were obtained when we

tried to investigate the excited-state relaxation behavior by introducing an additional delay time between the pump and the dump pulse. For the sake of a more intuitive interpretation of the final result, we therefore replace the propagators in the excited state by $U_Q(t-t')\delta(t-t')$ and $U_Q(t''-t''')\delta(t''-t''')$, respectively. The fourfold integral over time is then reduced to a twofold integral. Finally, taking advantage of the fact that the probe pulse does not temporally overlap with the pump and the Stokes pulses and that $T_{Pu} = T_{St}$, Eqn (6) can be recast in the form

$$\begin{aligned} P^{(3)}(\omega_{CARS}, T) = -\left(\frac{1}{i}\right)^3 e^{-i\mathbf{k}_{CARS}\mathbf{x}} \sum_{q''}\sum_{x'}\sum_{q'} e^{-iE_{x'}T}\langle\psi_0|\mu|q''\rangle \\ \times \int_{-\infty}^{\infty} dt\, f_{Pr}(t-T_{Pr}) e^{-i(E_{x'}+\omega^{\circ}_{Pr})(t-T_{Pr})} e^{i\omega_{CARS}t} \\ \times \langle q''|\mu|x'\rangle \int_{-\infty}^{\infty} d\,t' f_{Pu}(t''-T_{Pu}) f_{St}(t''-T_{Pu}) \\ \times e^{i(E_{x'}+\omega^{\circ}_{St}-\omega^{\circ}_{Pu})(t''-T_{Pu})}\langle x'|\mu|q'\rangle\langle q'|\mu|\psi_0\rangle + c.c. \end{aligned} \quad (7)$$

where T is defined as the delay time between the pump/Stokes pulse and the probe pulse, $T = T_{Pr} - T_{Pu}$. Equation (7) is now strongly reminiscent of electronic ground-state wave packet spectroscopy. The generation of the coherent superposition of vibrational modes is described within the last two lines, containing a time integral which is the Fourier transformation of the product of the pulse envelopes of the pump and the Stokes pulse with respect to $E_{x'} + \omega^{\circ}_{St} - \omega^{\circ}_{Pu}$. The integral is weighted with the product of Franck–Condon-type factors $\langle x'|\mu|q'\rangle\langle q'|\mu|\psi_0\rangle$ of the involved vibrational levels in $|X\rangle$ and $|Q\rangle$ during this stimulated Raman excitation process. The probing process at delay time T is described by the time integral in line 2 of Eqn (7), which with respect to ω_{CARS} is a Fourier transformation of a time function that contains the temporal pulse envelope of the probe pulse which oscillates with the anti-Stokes frequency $E_{x'} + \omega^{\circ}_{Pr}$. Here also matrix elements $\langle q''|\mu|x'\rangle$ that characterize the probe transition appear.

The experimentally detected spectrally dispersed transient CARS signal is proportional to the quantity

$$S(\omega_{CARS}, T) = |P^{(3)}(\omega_{CARS}, T)|^2 \quad (8)$$

We now rewrite Eqn (7) as

$$P^{(3)}(\omega_{CARS}, T) = \sum_{x'} e^{-iE_{x'}T} c(\omega_{CARS}, x') + c.c. \quad (9)$$

where the sum over the states q'' and q', the two time integrals, all Franck–Condon factors and all other constant factors are combined to the factor $c(\omega_{CARS}, x')$. Substitution of this expression into Eqn (8) finally yields an expression for the experimentally recorded transient CARS signal of the form

$$\begin{aligned} S(\omega_{CARS}, T) = \sum_{x'}\sum_{x''} \{ |c_1(x', x'')| \cos((E_{x'} + E_{x''})T + \varphi_{c_1}) \\ + |c_2(x', x'')| \cos((E_{x'} - E_{x''})T + \varphi_{c_2}) \} \end{aligned} \quad (10)$$

with constants $c_1(x', x'')$ and $c_2(x', x'')$ of the form

$$\begin{aligned} c_1(x', x'') &= |c_1(x', x'')| e^{i\varphi_{c_1}} = c(\omega_{CARS}, x') c(\omega_{CARS}, x'') \\ c_2(x', x'') &= |c_2(x', x'')| e^{i\varphi_{c_2}} = c(\omega_{CARS}, x') c^*(\omega_{CARS}, x'') \end{aligned} \quad (11)$$

As one might have expected, the final form of Eqn (10) now explicitly contains contributions that oscillate as a function of the pump–probe delay time T. The first term in the double sum of Eqn (10) oscillates with a periodicity that is given by the sum of two excited ground-state vibrational modes. This results in a fast beat pattern which, for the employed excitation wavenumbers, is beyond the time resolution of our experimental setup. However, the contributions in the second line oscillate with a frequency that is determined by the wavenumber differences of the coherently excited ground-state vibrational modes and should show up as strong beat patterns in the recorded transient signal. These beat frequencies can be extracted by applying a straightforward Fourier transformation to the time domain data yielding peaks at wavenumber positions $\tilde{\nu}_{FFT} = (1/2\pi c)(E_{x'} - E_{x''})$.

Summarizing the results of the theoretical derivation of this section which are relevant for the understanding of the experimentally detected signal, several points can be made. (i) Because of the pulse sequence and the resonance conditions that we employ, our fs-CARS measurements are performed in a pump and probe fashion, probing ground-state vibrational dynamics. (ii) According to Eqn (7), the excitation process consists of a stimulated Raman process for which the excitation bandwidth in the wavenumber domain is given by the Fourier transformation of the product of the pulse envelopes of the pump and the Stokes pulses. In our case of a large polyatomic molecule, this results in a simultaneous excitation of a multitude of vibrational states. (iii) The description of the probing process, given by the first time integral in Eqn (7), implies that every coherently excited molecular vibration ν_j contributes to the third-order polarization $P^{(3)}(\omega_{CARS}, T)$ with a bandwidth that is determined by the bandwidth of the probe pulse, centered at the wavenumber position $\tilde{\nu}_j = (1/2\pi c)(E_{x'} + \omega^{\circ}_{Pr})$. (Since it is clear that we are dealing with vibrational modes of the electronic ground state, in what follows the subscripts x' and x'' will be replaced by j and k, respectively.) In other words, the spectral width of the contribution of an individual mode to the detected CARS signal is given by the convolution of the Raman bandwidth of this mode with the spectral width of the probe pulse. (iv) According to Eqn (10), the experimentally detected transient CARS signal at every wavenumber position $\tilde{\nu}_{CARS}$ displays quantum beat patterns between vibrational modes contributing to the signal at this spectral position. Equations (7) and (10) also imply that the quantum beating of two modes is maximal approximately at the arithmetic mean wavenumber position of these modes. Using Fourier transform techniques to transform the two-dimensional time-domain data set $S(\tilde{\nu}_{CARS}, T)$ into a two-dimensional data set $S(\tilde{\nu}_{CARS}, \tilde{\nu}_{FFT})$, we are therefore able to

assign vibrational modes contributing to the signal and to extract spectral information on their relative wavenumber positions.

EXPERIMENTAL

The experimental setup of our fs-CARS spectrometer is similar to that described previously[11,12,27] and is only briefly discussed here. Pulses of about 90 fs duration centered at 800 nm from a Ti:sapphire oscillator (Mira, Coherent) are used as seed pulses for a regenerative amplifier (CPA-1000, Clark MXR) with a repetition rate of 1 kHz. The compressed amplified pulses with pulse energies of about 1 mJ and pulse durations of about 90 fs pump two optical parametric generators OPG (TOPAS, Light Conversion) with subsequent prism compressors. The two independent pulse trains are tunable over the visible spectral region and possess pulse durations of about 70 fs. Special care has been taken to minimize the residual chirp of these pulses by carefully analyzing the spectrally dispersed-detected non-Raman resonant transient CARS signal of a transparent solvent supplementary to the measurement of standard autocorrelation traces. This is necessary because we have found that chirp in either the pump or the Stokes pulses might greatly affect the distribution of excited vibrational modes in the sample. In our experiments, this effect can be adequately explained by the fact that the temporal pulse overlap of spectral components of the pump and the Stokes pulses is influenced when chirp is introduced.

One of the two OPG outputs is divided into two parts which serve as the pump and the probe pulses of equal wavelengths. The second OPG output is used for the red-shifted Stokes pulse. In order to be able to apply the desired pulse sequence in the measurement, two delay lines are needed. One is used to produce the temporal overlap of the pump and Stokes pulse which is fixed in the experiment. The second one provides the variable time delay for the probe pulse.

The detection setup for the coherently scattered anti-Stokes signal consists of a spectrometer (Spectra Pro-500, Acton) in which the signal is spectrally dispersed and a CCD camera (SDS 9000, Photometrics) for the simultaneous detection of all spectral components. The dispersed signal is recorded as a function of the probe pulse delay, resulting in a two-dimensional (CARS wavenumber $\tilde{\nu}_{CARS}$ and probe pulse delay time T) data set.

The wavelength arrangement for the investigated porphyrin systems (see Fig. 1) was chosen to achieve a strong resonance enhancement of the CARS process via excited electronic states. For the measurements on MgOEP and MgTPP the wavelengths of the pump/probe pulses were therefore tuned to the absorption maximum of the Q_{00} band. Together with a Stokes pulse wavelength that is determined by the required excitation wavenumber to excite modes of the porphyrin macrocycle, this results in a wavelength of the CARS signal in the vicinity of the Q_{01} absorption band maximum. For the OEP system, in which the two bands resulting from the transition into the degenerate Q state of the metalporphyrin systems split up in to a total of four bands, the wavelength of the pump pulse was tuned to coincide with the Q_x band, resulting in a CARS signal centered roughly at the position of the B_x band. The situation is exemplarily depicted in Fig. 2 for the excitation arrangement in MgOEP, together with its absorption spectrum.

As a spatial beam geometry for the CARS measurements we used the folded BOX-CARS configuration. The four light beams involved are spatially separated in this arrangement, allowing for background-free detection of the signal. Furthermore, the phase matching condition is fulfilled. The magic angle polarization scheme utilized in our CARS measurements was adopted from an experimental setup employed by Purucker *et al*.[10] The polarizations of the temporally overlapping pump and Stokes pulses are kept parallel in this arrangement, whereas the probe pulse is set to 60° and the CARS signal analyzer to −60° with respect to the pump/Stokes polarization directions.

The three investigated samples, MgOEP, MgTPP and OEP, were used as purchased (Porphyrin Products). All measurements were performed in solution, using a flow-type cuvette which was built from a rectangular glass capillary (Vitro Dynamics). As solvent we chose dichloromethane, because it possesses only weak vibrational bands in the excitation region and is relatively inert and non-polar compared with other solvents. Sample concentrations were adjusted to yield a linear absorption of typically 1.2 OD for the strongest Q band in a 1 mm pathlength cuvette. Sample integrity was monitored spectrophotometrically by recording absorption spectra of the sample prior to and after each time-resolved CARS measurement. No photodegradation was observed for the pulse energies employed of about 200 nJ for the pump and the probe pulse and about 300–400 nJ for the Stokes pulse.

In order to verify that solely vibrational dynamics of the porphyrin molecules are probed in the transient CARS studies, we regularly performed the same measurements on the pure solvent. In these measurements no dynamics from a Raman resonant scattering contribution of dichloromethane were observed.

EXPERIMENTAL RESULTS

Spectrally dispersed transient CARS signal

Figure 3 shows a typical spectrally dispersed transient CARS signal as a function of the probe pulse delay time T and the CARS wavenumber $\tilde{\nu}_{CARS}$. It was obtained from MgOEP dissolved in dichloromethane, for a pump and probe pulse wavelength of 580 nm and a Stokes pulse wavelength of 631 nm. The signal is centered at $\tilde{\nu}_{CARS} \approx 1400\ cm^{-1}$, corresponding to the mean excitation energy determined by the wavenumber difference of the pump and the Stokes

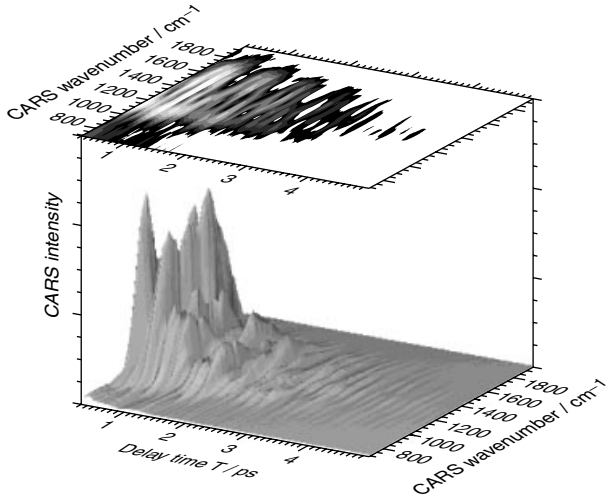

Figure 3. Typical spectrally dispersed-detected fs-CARS signal for MgOEP dissolved in dichloromethane for an excitation wavenumber in the spectral region of the modes of the MgOEP macrocycle. The signal lasts for about 4 ps and shows a complex oscillatory pattern, both in the direction of the wavenumber and the time axis, arising from the coherent excitation of a multitude of vibrational modes in this large molecular system.

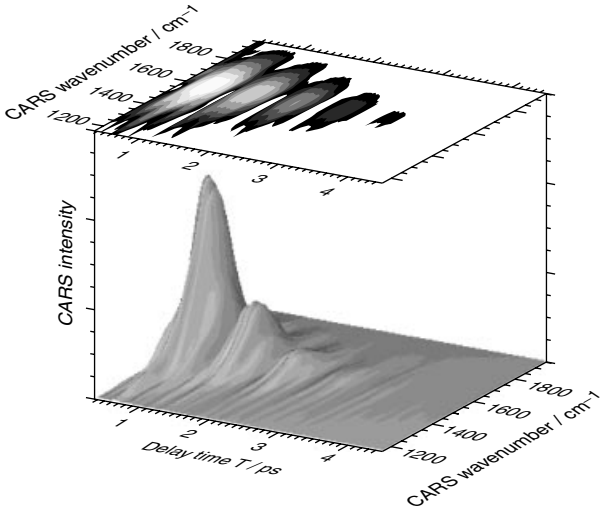

Figure 4. Spectrally dispersed-detected fs-CARS signal of MgOEP dissolved in dichloromethane for an excitation wavenumber of 1785 cm^{-1}. The signal shows a strong quantum beating between essentially only two excited vibrational modes of the MgOEP macrocycle with wavenumbers around 1580 cm^{-1}.

laser. It extends from $\tilde{\nu}_{CARS} \approx 1000$ to 1800 cm^{-1} and lasts for about 4 ps. The signal shows the expected oscillatory pattern for the high density of coherently excited normal modes in this system, with a strongly modulated structure in both the direction of the time axis and the wavenumber axis.

Before we move on to discuss the obtained transient CARS signals in more detail, we want to mention that a careful analysis of the data has shown that, although all the measurements were performed with the magic angle polarization geometry described above, there is still a residual non-Raman resonant scattering contribution to the transient signal around $T = 0$. We believe that it originates mostly form the influence of the optical Kerr effect on the polarization directions of the four light fields. Since this effect is not of interest to our investigations, we ensure that it is ignored in the data analysis by plotting and further analyzing only data obtained for delay times longer than 300 fs.

Returning to the discussion of the results obtained, we first want to illustrate that the complex structure of the transient CARS signal indeed originates from the large number of coherently excited modes in the investigated system. We also recorded a spectrally dispersed CARS transient for the same sample and the same pump/probe pulse wavelengths as in Fig. 3, but with a Stokes pulse wavelength of 647 nm. The chosen wavelength arrangement now corresponds to an excitation profile centered at about 1785 cm^{-1} and leads to an excitation of essentially only two vibrational modes with vibrational wavenumbers around 1600 cm^{-1}, lying in the wing of the excitation profile. The strongly reduced number of excited states for this Stokes pulse wavelength is due to the fact that MgOEP does not exhibit any resonance Raman-active modes above 1600 cm^{-1}. The raw data of the transient CARS signal for this excitation scheme are plotted in Fig. 4. It shows a relatively smooth CARS signal at $\tilde{\nu}_{CARS} \approx 1600\ cm^{-1}$ with essentially only one oscillation frequency of about 680 fs periodicity, possessing a very high contrast ratio. To analyze this signal further we calculated the power spectrum density (PSD) at every spectral position $\tilde{\nu}_{CARS}$ of the time domain signal using the fast Fourier transformation (FFT) method. Except for a subtraction of the exponentially decaying component of the transient signal which retains only oscillatory components and therefore removes the low-frequency component in the wavenumber domain data, no additional processing or smoothing of the data was performed. The PSD of the CARS transient of Fig. 4 is plotted in Fig. 5, as a function of $\tilde{\nu}_{CARS}$ and the FFT wavenumber $\tilde{\nu}_{FFT}$ resulting from the Fourier transformation procedure. It shows a strong peak at the CARS wavenumber $\tilde{\nu}_{CARS} = 1580\ cm^{-1}$ and the FFT wavenumber $\tilde{\nu}_{FFT} = 48\ cm^{-1}$, corresponding to the single oscillation frequency in the time domain signal. Recalling that the position of the peak along the CARS wavenumber axis is given approximately by the arithmetic mean wavenumber of two vibrational modes beating with each other and that the peak location along the FFT wavenumber axis corresponds to the wavenumber difference of the two modes, we can compare the peak position to the vibrational mode spectrum of MgOEP reported in the literature.[28] We thus attribute this peak to a quantum beating between the two modes ν_{10} and ν_{11}. Both of these modes possess b_{1g} symmetry and they are located at

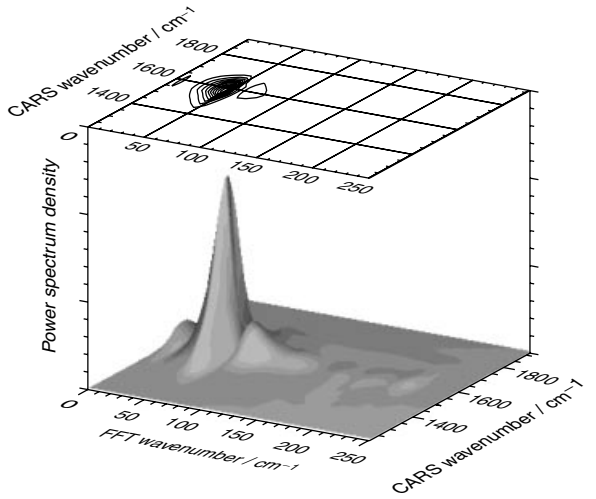

Figure 5. PSD of the transient CARS signal shown in Fig. 4, plotted as a function of the FFT wavenumber $\tilde{\nu}_{FFT}$ and the CARS signal wavenumber $\tilde{\nu}_{CARS}$. It shows a single strong peak at $\tilde{\nu}_{FFT} = 48$ cm^{-1} corresponding to the wavenumber difference of the two coherently excited modes ν_{10} and ν_{11}. The CARS wavenumber position of $\tilde{\nu}_{CARS} \approx 1580$ cm^{-1} corresponds approximately to the arithmetic mean of the spectral positions of the two modes. The two small features at $\tilde{\nu}_{FFT} = 6$ and 64 cm^{-1} indicate a weak contribution from a third mode.

wavenumber positions of 1606 and 1552 cm^{-1}, respectively. Taking a closer look at the PSD in Fig. 5, we can also identify two smaller peaks at FFT wavenumbers of 6 and 64 cm^{-1}. These peaks originate from the contribution of a third mode, ν_{19} at 1546 cm^{-1} with a_{2g} symmetry, and can be assigned to a weak beating between the modes ν_{11} and ν_{19}, and ν_{10} and ν_{19}, respectively. Furthermore, in the transient signal of Fig. 4 an additional beat frequency with a small amplitude and a periodicity of about 200 fs is apparent. We attribute this to a coherent superposition of a CH_2 scissor vibration and the porphyrin ring mode ν_{10}. This beat pattern, although clearly visible in the original transient signal, does not show up in the PSD of Fig. 5, indicating that the calculated PSD gives a rather conservative wavenumber domain picture of the quantum beat dynamics contained in the time domain CARS signal.

In conclusion, we note that the oscillatory structure of the time domain signal (Fig. 4) obtained for this wavelength arrangement where only a few modes are excited, together with the pronounced peaks in the wavenumber domain PSD plot (Fig. 5) from Fourier transformation, confirms a high signal-to-noise ratio and reproducibility achieved in our measurements. This finding is further supported by the fact that the excitation in this special case occurs within the wing, far away from the center of the excitation profile of the pump and the Stokes laser. It is now evident that the complex signal structure of the transient signal in Fig. 3 indeed originates from the fact that several vibrational levels are coherently excited and probed.

Spectrally dispersed CARS signals of MgOEP for different excitation wavenumbers

In order to obtain an overview picture of the ground-state vibrational dynamics in MgOEP, we performed spectrally dispersed-detected transient CARS measurements for a set of different excitation energies. The results obtained for a mean excitation wavenumber of 1785 cm^{-1} have already been discussed above. In this section we look at the situation where the mean excitation wavenumber of the stimulated Raman process has been tuned to about 1500 cm^{-1}, with a pump/probe pulse wavelength of 580 nm and a corresponding Stokes pulse wavelength of 635 nm. The excitation of a multitude of vibrational modes now leads to a strongly modulated transient signal similar to that shown in Fig. 3.

To investigate this complex signal structure we again employed Fourier transform methods and calculated the PSD of the time domain signal which is plotted in Fig. 6. Four relatively strong and two weaker peaks can be identified for an excitation wavenumber of 1500 cm^{-1}. Recalling the argument given above of how the position of a peak along the axis of $\tilde{\nu}_{FFT}$ and $\tilde{\nu}_{CARS}$ can be related to the spectral band positions of the two beating modes, we can now take full advantage of the two-dimensionality of the PSD plot and determine which modes of the vibrational spectrum of MgOEP contribute to the signal. The assignment of the excited modes is given in Table 1. It is interesting that the strong peak at $\tilde{\nu}_{FFT} = 48$ cm^{-1} and $\tilde{\nu}_{CARS} = 1580$ cm^{-1} appearing in Fig. 5 still exists, but has

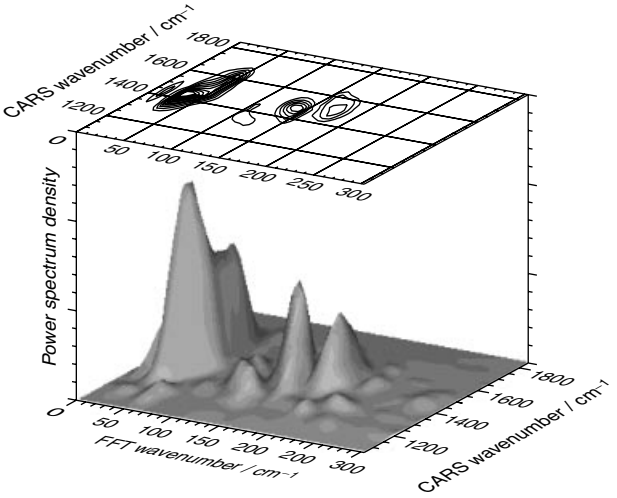

Figure 6. PSD of the spectrally dispersed transient CARS signal of MgOEP for an excitation wavenumber of $\tilde{\nu} = 1500$ cm^{-1}. Several quantum beatings between coherently excited modes can be identified, giving rise to a complex time domain signal which for this case is similar to that shown in Fig. 3. The assignment of the two separately identifiable stronger peaks and the double peak feature at $\tilde{\nu}_{FFT} \approx 45$ cm^{-1} which includes the strong peak from Fig. 5 is given in Table 1.

Table 1. Vibrational modes contributing to the fs-CARS signal of MgOEP at the three excitation wavenumbers, 1785, 1500 and 1350 cm^{-1} [a]

Excitation wavenumber/cm^{-1}	$\tilde{\nu}_{FFT}/cm^{-1}$	$\tilde{\nu}_{CARS}/cm^{-1}$	ν_k assignment	$\tilde{\nu}_k/cm^{-1}$	ν_j assignment	$\tilde{\nu}_j/cm^{-1}$	$\tilde{\nu}_j - \tilde{\nu}_k/cm^{-1}$
1785[b]	6	1580	$\nu_{19}(a_{2g})$	1546[e]	$\nu_{11}(b_{1g})$	1552[e,f]	6
	48	1570	$\nu_{11}(b_{1g})$	1552[e,f]	$\nu_{10}(b_{1g})$	1606[e,f]	54
	64	1600	$\nu_{19}(a_{2g})$	1546[e]	$\nu_{10}(b_{1g})$	1606[e,f]	60
1500[c]	10	1435	CH_2 scis	1434[f]	CH_2 scis	1440[g]	6
	36	1435	$\nu_{29}(b_{2g})$	1400[e,f]	CH_2 scis	1440[g]	40
	48	1580	$\nu_{11}(b_{1g})$	1552[e,f]	$\nu_{10}(b_{1g})$	1606[e,f]	54
	110	1370	$\nu_{21}(a_{2g})$	1317[e]	CH_2 scis	1434[f]	117
	140	1470	$\nu_{29}(b_{2g})$	1400[e,f]	$\nu_{19}(a_{2g})$	1546[e]	146
	175	1520	$\nu_{20}(a_{2g})$	1387[e,f]	$\nu_{11}(b_{1g})$	1552[f]	165
1350[d]	10	1435	CH_2 scis	1434[f]	CH_2 scis	1440[g]	6
	22	1210	$\nu_{13}(b_{1g})$	~1210[h]		—[i]	
	38	1435	$\nu_{29}(b_{2g})$	1400[e,f]	CH_2 scis	1440[g]	40
	50	1200	$\nu_{30}(b_{2g})$	~1160[j]	ν_{13}, (b_{1g})	~1210[h]	~50
	110	1370	$\nu_{21}(a_{2g})$	1317[e]	CH_2 scis	1434[f]	117
	140	1470	$\nu_{29}(b_{2g})$	1400[e,f]	$\nu_{19}(a_{2g})$	1546[e]	146
	175	1520	$\nu_{20}(a_{2g})$	1387[e,f]	$\nu_{11}(b_{1g})$	1552[f]	165

[a] The peak position along the FFT wavenumber ($\tilde{\nu}_{FFT}$) axis and along the CARS wavenumber ($\tilde{\nu}_{CARS}$) axis were extracted from the two-dimensional PSD plots of Figs 5–7 obtained from Fourier transformation of the time domain spectrally dispersed-detected CARS signal. Vibrational modes ν_k and ν_j giving rise to quantum beatings in the time domain signal according to their wavenumber differences were assigned by comparison with results from Refs 28–30 and 33.

[b] See Fig. 5.

[c] See Fig. 6.

[d] See Fig. 7.

[e] Assigned from ns-CARS data in Ref. 28.

[f] Assigned from resonance Raman data in Ref. 28.

[g] Assigned from Ref. 30.

[h] Estimated from the wavenumber differences $\Delta\tilde{\nu}$(NiOEP, MgOEP) for ν_{10} and ν_{19} in Refs 28 and 30. Both modes contain a $\delta(C_mH)$ component such as ν_{13}.

[i] There is no straightforward assignment possible. Except for the skeletal mode ν_{13} only CH_2 twisting modes (1250–1280 cm^{-1} for NiOEP in Ref. 30) are observed in this wavenumber region which are weak in Raman spectra under Q_0 resonance conditions. We therefore tentatively suggest a contribution from a combination band of the modes ν_3 and ν_{15}.

[j] Estimated from the ν_{30} position in NiOEP (1160 cm^{-1} in Ref. 30) and PdOEP (1166 cm^{-1}, larger radius).

now become a double peak feature together with a strong peak at $\tilde{\nu}_{FFT} = 36\ cm^{-1}$ and $\tilde{\nu}_{CARS} = 1435\ cm^{-1}$.

Even more modes contribute to the transient CARS signal if the mean excitation wavenumber is tuned to about 1350 cm^{-1}, as can be readily verified from the PSD plot depicted Fig. 7. The pump/probe wavelength was again set to 580 nm, amounting to a Stokes pulse wavelength of 629 nm in this measurement. The PSD now contains several strong and weak peaks. The strong peak from Fig. 5 is now absent because the excitation wavenumber is too low. Further, it is interesting that the two peaks at $\tilde{\nu}_{FFT} = 140\ cm^{-1}$, $\tilde{\nu}_{CARS} = 1470\ cm^{-1}$ and $\tilde{\nu}_{FFT} = 175\ cm^{-1}$, $\tilde{\nu}_{CARS} = 1520\ cm^{-1}$ from Fig. 6 are still existent but with lower intensity. Finally, there is another peak appearing in both Figs 6 and 7, at $\tilde{\nu}_{FFT} = 110\ cm^{-1}$ and $\tilde{\nu}_{CARS} = 1370\ cm^{-1}$. This peak is considerably stronger than in Fig. 6, a behavior which can also be explained by the reduced excitation energy employed in this measurement.

Table 1 gives a summarizing overview of all quantum beat features that are present in the PSD plots of the spectrally dispersed fs-CARS measurements on MgOEP dissolved in dichloromethane for the three different excitation wavenumbers. The assignment of these peaks to vibrational modes was performed by a comparison of our results with data obtained from resonance Raman measurements and ns-CARS experiments.[28,30] To this end we took advantage of the fact that the FFT wavenumber position of the peaks in the PSD plots directly corresponds to the wavenumber difference $\tilde{\nu}_j - \tilde{\nu}_k$ of modes ν_j and ν_k. This information allowed us to derive spectral information on the relative peak positions of individual vibrational modes from our measurements.

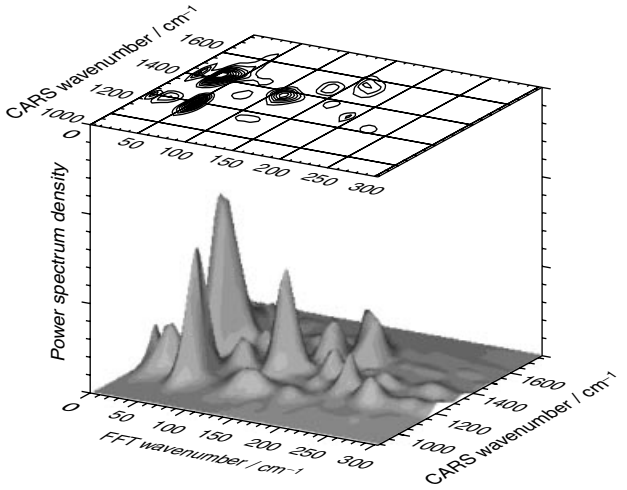

Figure 7. PSD of the transient CARS signal of MgOEP for an excitation wavenumber of 1350 cm^{-1}, indicating that a large number of modes is coherently excited in this measurement. The two-dimensionality of the data set again allows a determination of the contributing modes and yields information on their relative spectral positions (Table 1). It is interesting to note the change in intensities of the peaks that are present in both the PSD plots in Figs 6 and 7.

Vibrational dephasing

Femtosecond time-resolved CARS measurements allow a direct study of electronic ground-state vibrational relaxation of the investigated sample in real time. Although vibrational dephasing is not the main topic of this work, we nevertheless want to present a short report on the results that are readily available from our experiments.

Assuming that the overall intensity at a certain spectral position within the CARS signal is proportional to e^{-2T/T_2}, where T_2 is then to be seen as an average vibrational dephasing time of all modes contributing to the signal at this position, a fit to the transient signal of Fig. 3 yielded a dephasing time constant T_2 of 1360 ± 120 fs. This time constant is independent of the spectral position $\tilde{\nu}_{CARS}$. The large uncertainty of ± 120 fs has been estimated mainly by taking into account the strong oscillatory structure within the overall signal. Recalling that the contribution of every individual excited mode ν_j is maximum at its wavenumber position $\tilde{\nu}_j$ and has a spectral width that is equal to the one of the probe laser pulse [Eqn (7)], we can, as a rough approximation, infer that the vibrational relaxation of all excited modes occurs on a similar time-scale.

More accurate information about the dephasing times T_{2j} of individual modes ν_j can be derived from a more careful analysis of the spectral components of the dispersed CARS signal. By taking advantage of the information contained in the PSD we are able to determine which of the coherently excited modes contribute to the signal at certain spectral positions. We then make use of a theoretical description of fs-CARS which explicitly implies the relaxation behavior of the excited modes. In this formulation, and for the situation where the pulse durations of the laser pulses is considerably shorter than the dephasing times T_{2j}, the spectrally dispersed transient signal can be written as[6,7,25]

$$S(\omega_{CARS}, T) \propto \left| \sum_j Q_j e^{-\frac{T}{T_{2j}}} e^{-i(2\pi c\tilde{\nu}_j)T + i\varphi_j} \times \int_{-\infty}^{+\infty} dt\, E(t-T, \tilde{\nu}_j) e^{i\omega_{CARS}t} \right|^2 \quad (12)$$

where, Q_j denotes the coherent amplitude of mode ν_j which is proportional to the Fourier transform of the product of the two exciting pulses E_{Pu} and E_{St} with respect to the frequency mismatch of the jth mode, $\Delta\omega_j = \omega_{Pu} - \omega_{St} - 2\pi c\tilde{\nu}_j$. The electromagnetic field $E(t-T, \tilde{\nu}_j)$ describes the probe photons coherently scattered from mode ν_j. It is given by the amplitude of the probe pulse and its temporal pulse envelope and oscillates with $\omega_{Pr} + 2\pi c\tilde{\nu}_j$. Using Eqn (12) it is in principle possible to perform a numerical fit of the decay behavior at every wavenumber position $\tilde{\nu}_{CARS}$, where one might extract the vibrational dephasing times T_{2j} and also the amplitudes Q_j of all excited vibrational modes.

In order to show how this fitting procedure can be realized, we now want to concentrate on the measurement of MgOEP depicted in Fig. 4, with an excitation wavenumber of 1780 cm^{-1}. Owing to the special situation that only a few vibrational modes are covered by the excitation profile in this measurement, we obtain a manageable number of fit parameters and expect reliable and non-ambiguous results for the dephasing time constants T_{2j}. From the results obtained by the Fourier transformation of the transient signal (Fig. 5) and by the transient signal itself (Fig. 4), we infer that the CARS signal can, to a very good approximation, be described by a coherent superposition of the two modes ν_{10} and ν_{11}. In this case of only two excited modes, and if we are interested in the transient signal at a certain spectral position, Eqn (12) can be recast to the form[7]

$$S(T) \propto \hat{Q}_a^2 e^{-2\frac{T}{T_{2,a}}} + \hat{Q}_b^2 e^{-2\frac{T}{T_{2,b}}} + 2\hat{Q}_a\hat{Q}_b \cos[2\pi c(\tilde{\nu}_a - \tilde{\nu}_b)T + \Delta\varphi] e^{-\frac{T_{2,a}+T_{2,b}}{T_{2,a}T_{2,b}}T} \quad (13)$$

$\hat{Q}_j$ is now defined as the coherent amplitude Q_j times a scaling factor for the considered spectral position, determined by the Fourier integral in Eqn (12). The first two terms of Eqn (13) decay simply exponentially governed by the dephasing times $T_{2,a}$ and $T_{2,b}$ of the two contributing vibrational modes. The third term explicitly describes the oscillatory part in the signal and has generally a different decay behavior. Equation (13) allows a least-squares fit of the transient signal from which the quantities in which one is interested can be extracted. A similar approach has been proposed and used before to investigate terahertz beatings of two

or three coherently excited modes in neat liquids and binary mixtures of liquids of small molecules, where the contributing vibrational states were well known from the outset and the measurements were carried out without a spectrally dispersed detection of the transient CARS signal.[7]

For a first fit to the transient CARS signal using Eqn (13), we chose the spectral position of $\tilde{\nu}_{\mathrm{CARS}} = 1580\ \mathrm{cm}^{-1}$ (Fig. 8). This is the arithmetic mean wavenumber position of the two contributing modes, where the amplitudes $\hat{Q}_a$ and $\hat{Q}_b$ in this case are about the same. The two dephasing times that we obtain from this first fit procedure are $T_{2,a} = 964$ fs and $T_{2,b} = 1295$ fs. We further obtain an amplitude ratio $\hat{Q}_a/\hat{Q}_b$ of 1.07. In order to assign the two dephasing times to the vibrations ν_{10} and ν_{11}, we subsequently carried out the same fitting procedure at lower and higher wavenumbers (1450 and 1730 cm^{-1}), and took advantage of the fact that the relative amplitude of ν_{10} has to increase at higher wavenumbers and vice versa. Summarizing the results obtained from the two fitting procedures, two points can be made. First, the amplitude ratio shows the expected dependence, i.e. it increases for one direction and decreases in the other direction ($\hat{Q}_a/\hat{Q}_b = 1.25$ and 0.85). Second, the dephasing times that we obtained at these spectral positions support the finding that there is a difference of about 350 fs between $T_{2,10}$ and $T_{2,11}$. We were therefore able to assign the shorter decay time to mode ν_{10} and the longer one to ν_{11}, yielding $T_{2,10} \approx 960$ fs and $T_{2,11} \approx 1300$ fs.

Spectrally dispersed transient CARS measurements for MgTPP and OEP

In this section we present results obtained from spectrally dispersed transient CARS measurements on the two porphyrin systems magnesium tetraphenyl porphyrin (MgTPP) and octaethylporphyrin (OEP). MgTPP differs from the MgOEP system by having four phenyl substituents in the *meso* positions compared with the eight ethyl groups in the β-position of MgOEP. OEP is a free-base porphyrin possessing the same macrocycle and substituents as MgOEP, but is lacking the metal atom in the center, which is replaced by two hydrogen atoms (see Fig. 1).

Magnesium tetraphenylporphyrin

The excitation wavenumber for the measurement on MgTPP was set to 1400 cm^{-1}. With the same electronic resonance conditions as for the MgOEP, this corresponds to a pump/probe wavelength of 602 nm and a Stokes pulse wavelength of 657 nm. The PSD of the transient CARS signal is depicted in Fig. 9. It shows four clearly distinguishable peaks. The assignment of these quantum beat features to modes from the vibrational mode spectrum of MgTPP is given in Tables 2 and 3. The dephasing time T_2 of the transient signal, determined from a single exponential fit, consistently decreases from lower to higher excitation wavenumbers. At $\tilde{\nu}_{\mathrm{CARS}} = 1340\ \mathrm{cm}^{-1}$ we obtain $T_2 \approx 2070$ fs whereas at $\tilde{\nu}_{\mathrm{CARS}} = 1500\ \mathrm{cm}^{-1}$ we obtain $T_2 \approx 1700$ fs.

Octaethylporphyrin

The excitation wavenumber in the measurement on the octaethyl system has also been set to approximately 1400 cm^{-1}, corresponding to wavelengths of 570 nm for the pump/probe pulses and 619 nm for the Stokes pulse, using the electronic resonance condition described above (see Experimental section). The PSD of the spectrally dispersed transient CARS signal obtained in this measurement is shown in Fig. 10. Similarly to the measurements on

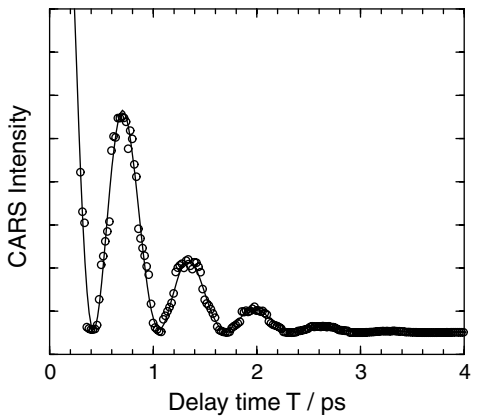

Figure 8. Least-squares fit to the transient CARS signal shown in Fig. 4 at a wavenumber position of 1580 cm^{-1}. The fit was performed using Eqn (13), assuming that only two modes contribute significantly to the signal which can be inferred from the PSD plot in Fig. 5. The fit yields two different vibrational dephasing times $T_{2,10} \approx 960$ fs and $T_{2,11} \approx 1300$ fs for the two modes $\tilde{\nu}_{10}$ and $\tilde{\nu}_{11}$, respectively.

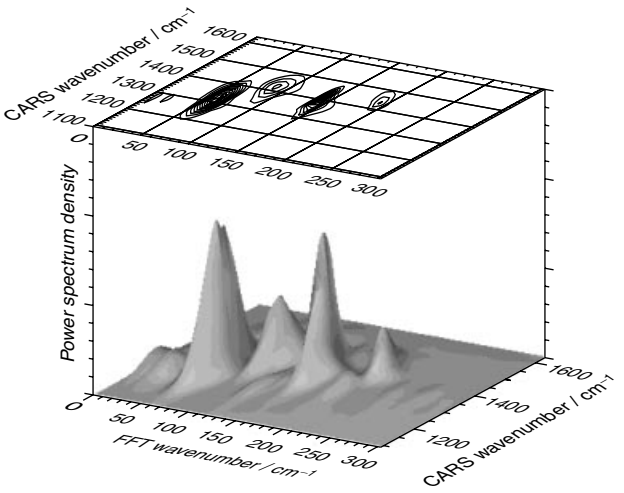

Figure 9. PSD plot for the spectrally dispersed fs-CARS signal obtained from MgTPP dissolved in dichloromethane for an excitation wavenumber of 1400 cm^{-1}. Four stronger peaks can be clearly identified. An assignment for the excited modes in this measurement is given in Table 3.

Table 2. MgTPP vibrational modes needed for the assignment of quantum beatings occurring in Fig. 9. (for comparison, modes of NiTPP are listed)[a]

ν_j	$\tilde{\nu}_j$(NiTPP)/ cm^{-1} [b]	$\tilde{\nu}_j$(MgTPP)/ cm^{-1}	$\Delta\tilde{\nu}_j$(Ni, Mg)/ cm^{-1}
$\nu_{11}(b_{1g})$	1504	1496[c]	8
$\nu_{12}(b_{1g})$	1302	[1262–1302][d]	[0–40]
$\nu_{20}(a_{2g})$	1341	[1301–1341][d]	[0–40]
$\nu_{27}(b_{2g})$	1269	[1229–1269][d]	[0–40]
$\nu_{28}(b_{2g})$	1485	[1445–1485][d]	[0–40]
$\nu_{29}(b_{2g})$	1377	[1337–1377][d]	[0–40]

[a] For NiTPP phenyl modes are observed only below 1200 and above 1500 cm^{-1} and were therefore excluded.[29]

[b] NiTPP modes taken from Refs 29, 31 and 32.

[c] The assignment of ν_{12} instead of ν_{11} in Ref. 33 is probably a misprint.

[d] Estimated values for MgTPP skeletal modes on the basis of the differences $\Delta\tilde{\nu}$ (Ni, Mg) of available modes.

MgOEP and MgTPP in this wavenumber regime, several peaks are clearly visibly. The assignment of these peaks to a quantum beating of the different contributing modes of the OEP is summarized in Table 4. The overall dephasing time we obtained by fitting the transient signal was $T_2 \approx 1720$ fs.

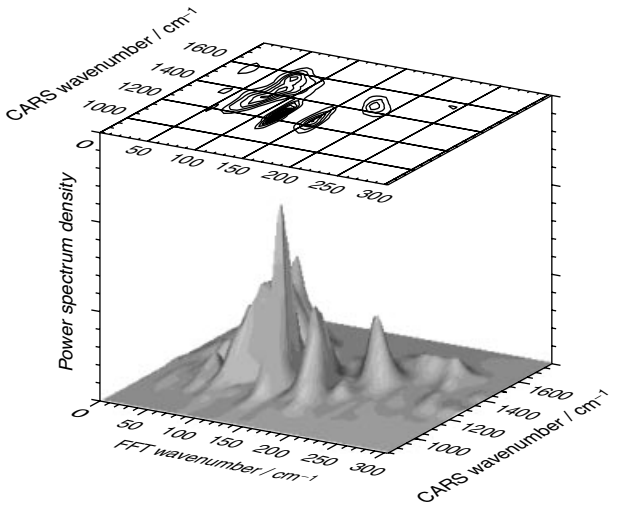

Figure 10. PSD plot of the spectrally dispersed transient CARS signal of OEP dissolved in dichloromethane for an excitation wavenumber of 1400 cm^{-1}. Five stronger peaks can be identified. The assignment of excited modes and their relative wavenumber positions are depicted in Table 4.

Table 3. MgTPP mode assignment for the FFT plot (Fig. 9) of the fs-CARS signal of MgTPP at an excitation wavenumber of 1400 cm^{-1} [a]

$\tilde{\nu}_{FFT}$/cm^{-1}	$\tilde{\nu}_{CARS}$/cm^{-1}	ν_k assignment	$\tilde{\nu}_k$/cm^{-1}	ν_j assignment	$\tilde{\nu}_j$/cm^{-1}	$\tilde{\nu}_j - \tilde{\nu}_k$/cm^{-1}
62	1310	$\nu_{27}(b_{2g})$	[1229–1269]	$\nu_{20}(a_{2g})$	[1301–1341]	[52–92]
88	1420	$\nu_{29}(b_{2g})$	[1337–1377]	$\nu_{28}(b_{2g})$	[1445–1485]	[88–128]
142	1410	$\nu_{20}(a_{2g})$	[1301–1341]	$\nu_{28}(b_{2g})$	[1445–1485]	[124–164]
192	1435	$\nu_{12}(b_{1g})$	[1262–1302]	$\nu_{11}(b_{1g})$	1496	[194–234]

[a] Mode assignment according to Table 2.

Table 4. Vibrational modes contributing to the fs-CARS signal of OEP at 1400 cm^{-1}, giving rise to the quantum beat structure as depicted in the FFT plot in Fig. 10

$\tilde{\nu}_{FFT}$/cm^{-1}	$\tilde{\nu}_{CARS}$/cm^{-1}	ν_k assignment	$\tilde{\nu}_k$/cm^{-1}	ν_j assignment	$\tilde{\nu}_j$/cm^{-1}	$\tilde{\nu}_j - \tilde{\nu}_k$/cm^{-1}
75	1500	$\nu_{28}(b_{1g})$	1478[a]	$\nu_{11}(a_g)$	1545[c]	67
80	1320	CH_2 twist	1276[b]	$\nu_{29}(b_{1g})$	1374[a]	98
				$\nu_4(a_g)$	1365[a]	89
120	1260	δ_s(NH)	1214[a]	$\nu_{26}(b_{1g})$	1327[a]	113
150	1285	$\nu_{13}(a_g)$	1160[a]	CH_2 wag	1316[b]	156
		δ_s(NH)	1214[a]	$\nu_4(a_g)$	1365[a]	151
180	1450	$\nu_{29}(b_{1g})$	1374[a]	$\nu_{11}(a_g)$	1545[c]	171
		$\nu_4(a_g)$	1365[a]			180

[a] Taken from trace C in Fig. 1 in Ref. 34; mode assignment according to Ref. 35.

[b] Taken from Ref. 30.

[c] Taken from traces A and B in Fig. 1 in Ref. 34.

DISCUSSION

We performed coherent anti-Stokes Raman scattering measurements of three different porphyrins in the time domain. By detecting the spectrum of the CARS signal we obtained two-dimensional plots which depict the scattered intensity as a function of the CARS wavenumber and the delay time between the pump and the probe pulse. A Fourier transformation converts the time domain signal into a two-dimensional spectrum which exhibits the power spectrum density as a function of the CARS and the FFT wavenumber. A peak in this spectrum represents the beating between two coherently excited modes of the investigated porphyrin system. The CARS wavenumber position is the average wavenumber value of the two beating modes which, owing to the spectral width of our laser pulses, contains an experimental error of approximately $\pm 50\ \mathrm{cm}^{-1}$. The FFT wavenumber value corresponds to the wavenumber difference between the beating modes. CARS and conventional stimulated resonance Raman spectroscopy are based on the same selection rules which are determined by the vibronic coupling matrix elements

$$c_{lm}^{\Gamma} = \langle l | \frac{\partial \hat{H}_{\mathrm{el}}}{\partial q^{\Gamma}} | s \rangle \tag{14}$$

where $|l\rangle$, $|s\rangle = Q_x$, Q_y, B_x, B_y represent the four electronic states of Gouterman's four-orbital model.[36] In metalporphyrins with a symmetric arrangement of peripheral substituents, Q_x, Q_y and B_x, B_y represent twofold degenerate states irrespective of the degree of non-planarity of the macrocycle. For MgOEP and MgTPP we can assume a planar macrocycle and thus a D_{4h} symmetry so that the states $|Q\rangle = |Q_x, Q_y\rangle$ and $|B_x, B_y\rangle$ exhibit e_u symmetry. The expression $\partial \hat{H}_{\mathrm{el}}/\partial q^{\Gamma}$ is the vibronic coupling operator of the Raman active vibration q, and Γ is the irreducible representation of this mode in a given point group.

For D_{4h} symmetry, group theory dictates that only normal modes of a_{1g}, a_{2g}, b_{1g} and b_{2g} symmetry can be resonance Raman active by vibronic coupling.[37] In conventional spontaneous resonance Raman scattering, Raman bands from a_{1g} modes are generally strong with B band excitation, due to their predominant Franck–Condon-type coupling contribution [$l, m = B_x, B_y$ in Eqn (14)]. In contrast a_{2g}, b_{1g} and b_{2g} modes gain most of their intensity from Herzberg–Teller coupling between Q and B states so that they dominate the spectra obtained with Q band excitation.[37,38] However, bands from a_{1g} modes are still contributing to the Q band spectra owing to strong Q state Franck–Condon coupling.[39,40]

The free base porphyrin OEP possesses a D_{2h} symmetry for which the degeneracies of $|Q\rangle$ and $|B\rangle$ are lifted. The split is particularly large for the Q states. The symmetries of the excited states are therefore b_{3u} for Q_x and B_x and b_{2u} for Q_y and B_y. The Raman-active modes transform like a_g, b_{1g}, b_{2u} and b_{3u}. Thus, modes possessing e_u symmetry in D_{4h} porphyrins are now resonance Raman active, since this representation splits into b_{2u} and b_{3u} in the lower symmetry of the free-base porphyrins.[35]

In the absence of any higher order multimode mixing effects,[40] the spontaneous resonance Raman intensity of a porphyrin vibration is proportional to the square of the weighted sum

$$I\left(q^{\Gamma}\right) \propto \left[\sum_{l,m} c_{lm}^{\Gamma}\left(q^{\Gamma}\right) f_{lm}\left(q^{\Gamma}\right)\right]^2 \tag{15}$$

where f_{lm} is a complicated function which depends on electronic transition dipole moments and the excitation wavenumber. Equation (15) reflects the coherent superposition of scattering amplitudes in the excited states. Hence, in resonance Raman scattering one obtains a coherent excitation of different vibronic states. Since, however, the emission process is spontaneous, the excitation of the (final) vibrational sates in the electronic ground state is incoherent.

In the present CARS experiment the interaction with the red-shifted Stokes pulse yields an induced emission which creates a coherent excitation of vibrational states in a wavenumber region defined by the wavelength and the width of the pump and the Stokes pulse. The latter can be tuned so that different parts of the normal mode spectrum can be excited. The excited vibrational states are probed by anti-Stokes scattering, which in our experiment is in resonance with the first excited Q state $\left(|Q_{x,y}, 1\rangle\right)$. The close proximity of other vibronic states and intensive vibronic coupling with vibronic B states again gives rise to a coherent superposition of scattering amplitudes from various vibronic states. Hence, in terms of the vibronic coupling parameters in Eqn (14), the CARS intensity is now proportional to the more complicated expression

$$I \propto \left(\sum_{q}\sum_{l,m}\sum_{l',m'} c_{lm}^{\Gamma}\left(q^{\Gamma}\right) f_{lm}\left(q^{\Gamma}\right) c_{l'm'}^{\Gamma}\left(q^{\Gamma}\right) f_{l'm'}\left(q^{\Gamma}\right) F_{\mathrm{St}}\right)^2 \tag{16}$$

where $l, m, l', m' = Q_x, Q_y, B_x, B_y$. The sum $\sum_q$ runs over all Raman-active modes, but their contribution is limited by the spectral profile F_{St} of the Stokes pulse.

Equation (16) describes the intensity of steady-state CARS experiments. In the present study, the probe pulse is delayed with respect to pump/Stokes pulse in order to monitor the dynamics of the excited vibrational coherence. In the Fourier transformed data we obtained signals resulting from the beating of two normal modes, the frequencies of which are in the range of the sum of the bandwidths of the pump and Stokes pulse. The intensities of these features are proportional to the corresponding coherent amplitudes [Eqn (13)]. This can be expressed in terms of the vibronic coupling matrix elements as follows:

$$Q_a Q_b \propto \left[\sum_{l,m}\sum_{l',m'}\sum_{r,s}\sum_{r',s'} c_{lm}^{\Gamma_a}\left(q_a\right) f_{lm}\left(q_a\right) c_{l'm'}^{\Gamma_a}\left(q_a\right) \times f_{l'm'}\left(q_a\right) c_{rs}^{\Gamma_b}\left(q_b\right) f_{rs}\left(q_b\right) c_{r's'}^{\Gamma_b}\left(q_b\right) f_{r's'}\left(q_b\right)\right] F_{\mathrm{St}} \tag{17}$$

Equation (17) displays a complex relationship between the transient CARS signal intensity and the corresponding spontaneous resonance Raman intensities. It is therefore not possible to deduce the transient signal intensity directly from the spontaneous Raman spectrum. In fact, a beating originating from a weak and a strong mode in the Raman spectrum might yield a significant transient CARS signal. However, a somewhat general and qualitative prediction can be made owing to the following consideration. It is well known that the (spontaneous) Q band Raman scattering of a_{1g}, b_{1g} and b_{2g} modes is determined by the strength and the sign of interstate Herzberg–Teller (c^{Γ}_{QB}, c^{Γ}_{BQ}) and intrastate Franck–Condon or Jahn–Teller (c^{Γ}_{QQ}) coupling. In contrast, a_{2g} modes are only Herzberg–Teller active ($c^{a_{2g}}_{QQ} = 0$).[38] Equation (17) suggests that the beating of two modes which exhibit strong contributions from both types of coupling give rise to the strongest oscillatory behavior in the transient CARS signal. If this criterion is valid, results from earlier resonance Raman dispersion spectroscopy experiments on various Ni(II)-porphyrins[39,40] suggest that the intensity of the transient signals should roughly follow the following order with respect to the symmetry of the beating modes:

$$b_{1g} + b_{1g} > b_{1g} + b_{2g} > b_{1g} + a_{2g} > a_{2g} + a_{2g} > b_{2g} + a_{2g} > b_{2g} + b_{2g} > b_{1g} + a_{1g} > b_{2g} + a_{1g} > a_{2g} + a_{1g} > a_{1g} + a_{1g} \quad (18)$$

A comparison of the assignments of the transient signals in Table 1–3 and their intensities in Figs 5–7, 9 and 10 shows that this prediction is in qualitative agreement with some of our observations. Figure 5 shows that the signal of the two b_{1g} modes ν_{10} and ν_{11} is much more intense than the two peaks containing the a_{2g} symmetric ν_{19} mode. In Fig. 6 the $\nu_{10} + \nu_{11}$ signal is only exceeded by the peak from the ν_{29} and the CH_2 scissor vibration. The CH_2 scissor mode is assignable to four nearly degenerate vibrations of a_{1g}, b_{1g}, b_{2g} and a_{2g} symmetry. The signals of the combinations $\nu_{29}(b_{2g}) + \nu_{19}(a_{2g})$ and $\nu_{20}(a_{2g}) + \nu_{11}(b_{1g})$ are less intense but still significant. Apart from the ν_{11} mode there is no other b_{1g} symmetric macrocycle mode in the wavenumber range of Fig. 6. The PSD in Fig. 7 is dominated by a signal at a CARS wavenumber of 1210 cm^{-1}. One of the contributing modes is certainly the ν_{13} at 1213 cm^{-1}, but the identity of the second mode is unclear. In NiOEP the next b_{1g}-type mode is at 1131 cm^{-1},[30] but this is inconsistent with the very small wavenumber difference of 22 cm^{-1}. Since no fundamental modes are in the close proximity of the ν_{12} mode, one may instead invoke an interaction with a combination tone. Possible candidates for the respective fundamentals are difficult to identify because they must not be Raman active. The second very intense signal was assigned to $\nu_{30}(b_{2g}) + \nu_{13}(b_{1g})$. The peak which shows the third highest intensity results from the $\nu_{21}(a_{2g})$ and the CH_2 scissor vibration.

In the corresponding spectrum of MgTPP in Fig. 9, the two strongest signals originate from the combinations $\nu_{27}(b_{2g}) + \nu_{20}(a_{2g})$ and $\nu_{20}(a_{2g}) + \nu_{28}(b_{2g})$. The peak which is assigned to the combination of the two b_{1g} modes ν_{12} and ν_{11} is weaker. This seems to contradict the above prediction [Eqn (13)]. However, the ν_{12} mode is generally a very weak band which is barely detectable in the spontaneous resonance Raman spectrum. Hence the weak coupling strength of the ν_{12} mode is compensated by the strong vibronic coupling capability of the ν_{11} mode.[39,40] In accordance with Eqn (13), a_{1g} modes do not contribute to any of the obtained intense signals.

It should be mentioned that the polarization conditions employed in the experimental setup favor contributions from a_{1g} modes relative to those of b_{1g} and b_{2g} modes. In spite of this bias, the latter contribute significantly to all transients, thus supporting the prediction of Eqn (18).

For the free-base OEP other selection rules apply and vibronic coupling contributions to the transient CARS signal follow rules different from those for metalporphyrins. In principle, modes of all Raman-active symmetries can generate intense signals. However, modes of b_{2u} and b_{3u} symmetry are less likely to have an impact, because they correspond to e_u modes in D_{4h} which are not Raman active. Indeed, modes of these symmetries do not show up in Table 4.

CONCLUSION

Spectrally dispersed fs time-resolved CARS was applied to investigate the electronic ground-state vibrational dynamics of three different porphyrin systems. We have shown that this method provides a valuable tool for the investigation of the complex dynamics of a coherent superposition of a great number of vibrational modes in large polyatomic molecules, excited simultaneously by spectrally broad pulses inherent to sub-picosecond time-resolved spectroscopy. From the recorded two-dimensional data one obtains the dephasing behavior and spectral information on the individual normal modes at the same time. As a key procedure for a thorough understanding of the complex transient signal, and a disentanglement of the contributing modes, Fourier transformations of the time domain signal were employed.

In the MgOEP system, a broad spectral range in the region of the porphyrin macrocycle modes was investigated with different excitation wavenumbers. The results obtained yield detailed information on the relative spectral positions of a large number of modes which is complementary to data that have been available from spectrally resolved (cw) spectroscopic techniques. Furthermore, the different real-time dephasing behavior of two ring modes in this congested spectral region has been accurately determined, yielding results that are not readily available from the bandwidths of spontaneous Raman lines or comparable spectral data.

According to the structural differences of MgTPP and OEP, we obtain distinctly different quantum beat features for these molecules compared with those of MgOEP, as a consequence of shifted band positions and the fact that the

contribution of individual modes to the CARS signal varies strongly for the three systems.

Acknowledgments

Financial support from the Deutsche Forschungsgemeinschaft and from the Sonderforschungsbereich 347, Teilprojekt C2 and C5, is gratefully acknowledged. T. Chen expresses his thanks to the Volkswagenstiftung for a scholarship. S. Schlücker thanks the Stiftung Stipendien-Fonds des Verbandes der Chemischen Industrie and the Bundesministerium für Bildung und Forschung for support. We also acknowledge financial assistance from the Fonds der Chemischen Industrie.

REFERENCES

1. Zewail AH. *Femtochemistry: Ultrafast Dynamics of the Chemical Bond*, vols I and II. World Scientific: Singapore, 1994.
2. Sundström V (ed.). *Femtochemistry and Femtobiology: Ultrafast Reaction Dynamics at Atomic-scale Resolution*. Nobel Symposium 101. Imperial College Press: London, 1996.
3. Zewail AH. *J. Phys. Chem. A* 2000; **104**: 5660.
4. Kaiser W (ed.). *Ultrafast Laser Pulses and Applications*. Springer: Berlin, 1988.
5. Manz J, Wöste L (eds). *Femtosecond Chemistry*, vols I and II. VCH: Weinheim, 1995.
6. Leonhardt R, Holzapfel W, Zinth W, Kaiser W. *Chem. Phys. Lett.* 1987; **133**: 373.
7. Leonhardt R, Holzapfel W, Zinth W, Kaiser W. *Rev. Phys. Appl.* 1987; **22**: 1735.
8. Fickenscher M, Laubereau A. *J. Raman Spectrosc.* 1990; **21**: 857.
9. Li W, Purucker H-G, Laubereau A. *Opt. Commun.* 1992; **94**: 300.
10. Purucker H-G, Tunkin V, Laubereau A. *J. Raman Spectrosc.* 1993; **24**: 453.
11. Schmitt M, Knopp G, Materny A, Kiefer W. *Chem. Phys. Lett.* 1997; **270**: 9.
12. Siebert T, Schmitt M, Michelis T, Materny A, Kiefer W. *J. Raman Spectrosc.* 1999; **30**: 807.
13. Lozovoy VV, Grimberg BI, Brown EJ, Pastrik I, Dantus M. *J. Raman Spectrosc.* 2000; **31**: 41.
14. Knopp G, Pinkas I, Prior Y. *J. Raman Spectrosc.* 2000; **31**: 51.
15. Lang T, Motzkus M. *J. Raman Spectrosc.* 2000; **31**: 65.
16. Meyer S, Schmitt M, Materny A, Kiefer W, Engel V. *Chem. Phys. Lett.* 1997; **281**: 332.
17. Meyer S, Schmitt M, Materny A, Kiefer W, Engel V. *Chem. Phys. Lett.* 1998; **287**: 753.
18. Meyer S, Engel V. *J. Raman Spectrosc.* 2000; **31**: 33.
19. Tannor DJ, Rice SA, Weber PM. *J. Chem. Phys.* 1985; **83**: 6158.
20. Okamoto H, Yoshihara K. *Chem. Phys. Lett.* 1990; **172**: 323.
21. Kamalov VF, Svirko JP. *Chem. Phys. Lett.* 1992; **194**: 13.
22. Pausch R, Heid M, Chen T, Kiefer W. *J. Chem. Phys.* 1999; **110**: 9560.
23. Heid M, Chen T, Pausch R, Schwoerer H, Kiefer W. *J. Chin. Chem. Soc.* 2000; **47**: 637.
24. Chen T, Vierheilig A, Waltner P, Heid M, Kiefer W, Materny A. *Chem. Phys. Lett.* 2000; **326**: 375.
25. Heid M, Chen T, Schmitt U, Kiefer W. *Chem. Phys. Lett.* 2001; **334**: 119.
26. Laubereau A, Kaiser W. *Rev. Mod. Phys.* 1978; **50**: 607.
27. Schwoerer H, Pausch R, Heid M, Engel V, Kiefer W. *J. Chem. Phys.* 1997; **107**: 9749.
28. Nissum M, Funk J-M, Kiefer W. *J. Raman Spectrosc.* 1999; **30**: 605.
29. Li XY, Czernuszewicz RS, Kincaid JR, Su YO, Spiro TG. *J. Phys. Chem.* 1990; **94**: 31.
30. Li XY, Czernuszewicz RS, Kincaid JR, Stein P, Spiro TG. *J. Phys. Chem.* 1990; **94**: 47.
31. Unger E, Dreybrodt W, Schweitzer-Stenner R. *J. Phys. Chem. A* 1997; **101**: 5997.
32. Rush TS, Kozlowski PM, Piffat CA, Kumble R, Zgierski MZ, Spiro TG. *J. Phys. Chem. B* 2000; **104**: 5020.
33. Kim D, Terner J, Spiro TG. *J. Am. Chem. Soc.* 1986; **108**: 2097.
34. Sato S, Aoyagi K, Haya T, Kitagawa T. *J. Phys. Chem.* 1995; **99**: 7766.
35. Li XY, Zgierski MZ. *J. Phys. Chem.* 1991; **95**: 4268.
36. Gouterman M. *J. Chem. Phys.* 1959; **30**: 1139.
37. Spiro TG, Strekas TC. *J. Am. Chem. Soc.* 1974; **96**: 338.
38. Shelnutt JA, Cheung L, Chang RCC, Yu NT, Felton RH. *J. Chem. Phys.* 1977; **66**: 3387.
39. Unger E, Bobinger U, Dreybrodt W, Schweitzer-Stenner R. *J. Phys. Chem.* 1993; **97**: 9956.
40. Schweitzer-Stenner R, Stichternath A, Dreybrodt W, Jentzen W, Song ZP, Shelnutt JA, Faurskov-Nielsen O, Medforth CJ, Smith KM. *J. Chem. Phys.* 1997; **107**: 1794.